ACQUISITION AND DOCUMENTATION OF VESSELS USING HIGH-RESOLUTION 3D-SCANNERS

Hubert Mara, Julia Portl

1 INTRODUCTION

Since the late 1980ies, 3D-acquisition has steadily become a standard tool for various archaeological applications.[1] The work described in this chapter is focused on the documentation of small objects using optical 3D-scanners; these can easily be applied in everyday work and in many ways can be handled just as a camera. This includes a steep learning curve for the use of the 3D-scanner.

The most prominent optical methods are stereo and/or structured light.[2] The latter can also be realized using a laser with visible light as used for the CVA volume Austria 5. However it should not be called laser scanner, as this term is widely related to so-called airborne and terrestrial laser scanners used for landscape surveys and the documentation of architecture.[3] These 3D-scanners use the principle of Time-Of-Flight (TOF)[4] and are not suitable for small archaeological finds. Therefore, projects in architecture with details such as reliefs require the combination of both types of 3D-scanners.[5] Another important method for the 3D-documentation of small objects such as vessels and fragments is Computed Tomography, which is covered in Chapter 4 and 5.

While the Austrian CVA project is our main application-orientated project in Roman and Greek archaeology, we have a comprehensive variety of projects within other areas of cultural heritage, demonstrating the versatility of new methodologies using data from close-range 3D-scanners on very different types of objects:

Extraction of cuneiform characters from clay tablets[6]
Weathered Angkor style bas-reliefs in Cambodia[7]
Medieval column capitals[8]
Multispectral 3D analysis of frescoes in Pompeii[9]

[1] C. Steckner, SAMOS: Dokumentation, Vermessung, Bestimmung und Rekonstruktion von Keramik, in: Akten des XIII. Internationalen Kongresses für Klassische Archäologie. Berlin, 24.–30. Juli 1988 (Mainz 1990) 631–635; C. Steckner, Das SAMOS Projekt, AiD 5 (1), 1989, 16–21.

[2] R. Sablatnig – C. Menard, Stereo and Structured Light as Acquisition Methods in the Field of Archaeology, in: S. Fuchs – R. Hoffmann (ed.), Mustererkennung '92, 14. DAGM-Symposium Dresden (Berlin 1992) 398–404.

[3] M. Rutzinger – B. Höfle – N. Pfeifer, Object-Based Image Analysis, in: Object detection in airborne laser scanning data – an integrative approach on object-based image and point cloud analysis (Berlin 2008) 645–662.

[4] I. Moring – T. Heikkinen – R. Myllyla – A. Kilpela, Acquisition of three-dimensional image data by a scanning laser rangefinder, Optical Engineering 28, 1989, 897–905.

[5] U. Quatember – B. Thuswaldner – R. Kalasek – C. Bathow – B. Breuckmann, The Virtual and Physical Reconstruction of the Octagon and Hadrian's Temple in Ephesus, in: H. G. Bock – W. Jäger – H. Mara – M. Winckler (ed.), Proc. 2nd Workshop on Scientific Computing for Cultural Heritage (SCCH), Heidelberg, Germany, 2009 (Berlin 2012) 217–228.

[6] Mara et al., GigaMesh.

[7] A. Schäfer – H. Mara – J. Freudenreich – S. Krömker – H.-G. Bock, Visualization and Documentation of Weathered Bas-Reliefs using Close-Range 3D-Scanners, in: Proc. of 7th International Conference on Science and Technology in Archaeology and Conservation Workshop on Documentation and Conservation of Stone deterioration in Heritage Places (CIPA/ICOMOS), Petra, Jordan, 2010 (in print).

[8] G. Christ – H. Mara – O. Wagener, Ein altes Kapitell in neuen Ansichten – die Möglichkeiten des 3D-Scannings am Beispiel eines Kapitells der pfälzischen Burg Anebos, Burgen und Schlösser 51(1), 2010, 51–52.

[9] H. Mara – B. Breuckmann – C. Lang-Auinger, Multi-Spectral High-Resolution 3D-Acquisition for Rapid Archaeological Documentation and Analysis, in: Proc. of 17th European Signal Processing Conference (EUSIPCO '09), Glasgow, Scotland, United Kingdom, 2009 (2009) 1205–1209.

Worn Greek inscriptions in Ephesos[10]

Analysis of the manufacturing technique of Nasca pottery.[11]

For these projects, it was not possible to use so-called low-cost 3D-scanners, e.g. the *DAVID Laserscanner*[12] from the Braunschweig University of Technology. Such 3D-scanners are very valuable for experiments and teaching purposes, but they are not cost-effective for the documentation of larger quantities of objects, because they do not provide accurate data[13] for our documentation purposes. This and the lack of a robust, flexible and user friendly setup of low-cost 3D-scanners dramatically increases the time for acquisition and post-processing. As the access to objects within a museum is usually limited by a strict time-frame, the acquisition has to be done as fast and as accurate as possible by experienced persons. For the CVA projects, we typically had three to four working weeks available for more than 100 objects. This means that each object had to be properly acquired in approximately one hour. Furthermore, there is usually no chance to return to the museum at a later time to repeat the acquisition. Having experienced persons operating the 3D-scanner adds personnel and travel cost to the true cost of 3D-acquisition and any savings by using a low-cost 3D-scanner would not compensate these costs.

The next section describes the 3D-scanners and their setup used for the recent CVA volumes of the KHM. Section 3 shows the method for the computation of the profile line, the lateral views and rollouts used as a basis for the final publication. Afterwards, we describe the volume estimation for transport vessels as well as for vessels with special compartments (Einsatzbehälter). Finally, a summary and an outlook are given.

2   3D-ACQUISITION – PRINCIPLES AND SETUP

Regarding the positive results from our previous projects, we chose an optical 3D-scanner for the data acquisition for the CVA volumes in Vienna. Such a 3D-scanner consists of one or more digital cameras. Therefore, most of the rules from photography apply, such as shutter time and depth of field. Images from 3D-scanners are called range images, as the gray value of a pixel represents the distance to the surface of the scanned object. The gray values – typically in the range of [0 … 255] – are mapped to an absolute distance (e.g. mm). This means that the 3D-scanner can only acquire surfaces in its *Field of View* (*FOV*) and range images have to be registered (stitched together) in order to receive a 3D-model. The optics of the scanner also has a depth of field defining a focal plane, which defines the so-called working distance. This is typically a fixed distance, because optics with a fixed focal length is used to avoid moving parts, as these can lower the accuracy of the measurements.

The differences to photography are: per definition we have two *FOV*s, where one is from a camera and the second is either from a camera (stereo) or a light source (structured light). Both *FOV*s have to overlap as shown in Figure 1, defining the 3D-scanner's *FOV*. The pyramid frustum shown in green color is the space $(x_{min}, y_{min}, z_{min}, x_{max}, y_{max}, z_{max})$ in which an object can be acquired. For practical reasons, the range image diagonal (top surface of the pyramid, *FOV* in mm) is given by the manufacturers of the 3D-scanner, instead of the focal length of the optics. Most of the 3D-scanners use a camera to acquire color or grayscale information of the surface of the object, which is then used as a texture-map for the 3D-models. This influences the setup of the illumination, because we want to avoid shadows as we can compute them later and do not want them permanently in the texture-map.

[10]   R. Kalasek – H. Mara – H. Taeuber, Reading Weathered Ancient Laws in 3rd Dimension, in: 13. Int. Tagung: Kulturelles Erbe und Neue Technologien, Vienna, Austria, November 2008 (oral presentation).

[11]   H. Mara, Pottery plotted by Laser – 3D-Acquisition for Documentation and Analysis of Symmetry of Ancient Ceramics, in: M. Reindel (ed.), New Technologies for Archaeology – Multidisciplinary Investigations in Palpa and Nasca, Peru (Berlin 2008) 379–408.

[12]   S. Winkelbach – S. Molkenstruck – F. M. Wahl, Low-Cost Laser Range Scanner and Fast Surface Registration Approach, in: Proc. of 28th DAGM symposium, Berlin, Germany, September 12–14, 2006, Lecture Notes in Computer Science 4174 (Berlin 2006) 718–728.

[13]   C. Bathow – B. Breuckmann – R. Scopigno, Verification and Acceptance Tests for High Definition 3D Surface Scanners, in: A. Artusi (ed.), Proc. VAST International Symposium on Virtual Reality, Archaeology and Cultural Heritage, Palais du Louvre, Paris, France, 2010 (Goslar 2010) 9–16.
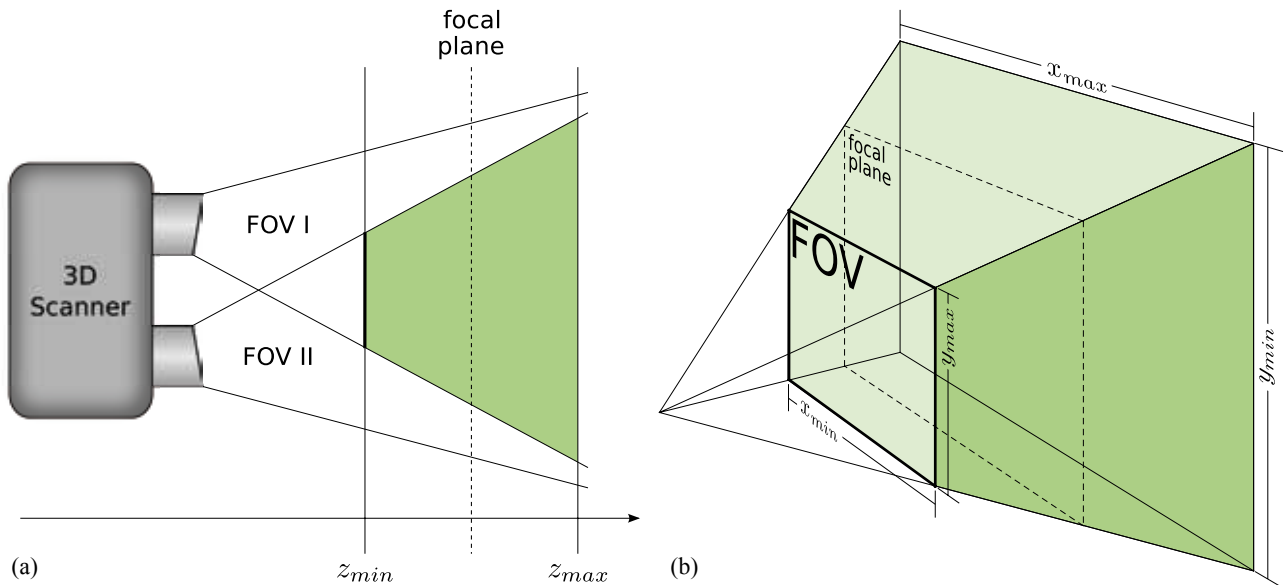
Figure 1: (a) Side view of the scheme of an optical 3D-scanner and its *Field of View*. The scheme is valid for stereo and for structured light. FOV I is the field of view of camera 1. FOV II is either the field of view of camera 2 (stereo) or the projection of structured light. The area in green shows the frustum of the overlapping areas defining the volume in which an object can be acquired. (b) Perspective drawing of the FOV and its dimensions.

2.1 Resolution and Features of Optical 3D-Scanners

Choosing a 3D-scanner for a project is like choosing any other measuring device and is based on several key factors, such as accuracy in respect to your application, user friendly handling, and a flexible but robust setup. For the two CVA projects in Vienna, a *Konica-Minolta Vi-9i* was used for the work done in 2006 and a *Breuckmann smartSCAN-3D-HE* for the follow-up project in 2009. Both 3D-scanners belong to working groups (see Acknowledgements) at Universities with a project focus on developing new methods for Cultural Heritage. Therefore, they were chosen to be used in this specific field, but also to be as versatile and as accurate as possible. In hindsight, a 3D-scanner tailored for a CVA project would be a device with a higher accuracy than the one in 2006 and a less expensive configuration than of the 3D-scanner in 2009. However, the key features for a successful use of both devices were:

Handling could be done by either moving the 3D-scanner, which can be mounted on a standard tripod, around the object or vice versa. Additionally, a *turntable* was available to decrease acquisition time, as shown in the next section.

Accuracy was provided sufficiently for archaeological line drawings to be computed from 3D-models, considered to have an accuracy lower than 0.1 mm.

Flexibility for objects of different sizes: The smallest object was a fragment of a ceramic[14] having a surface of ≈ 1 cm², while the largest objects[15] had a height and/or diameter of ≈ 60 cm.

Color acquisition by the 3D-scanner itself. This is a rather rare option, because for this there is usually no demand in the industrial field and therefore 3D-scanner manufacturers do not provide it. The alternative of adding photographs is very time consuming and not practicable under our time constraints.

Accuracy and flexibility depend on the choice and type of optics of the 3D-scanner. To achieve this, both 3D-scanners had interchangeable optics, which can be classified as tele/macro, middle and wide in general – details are shown below. The tele/macro optics provides the highest resolution, but the acquired area will be the smallest. The wide-angle optics provides the contrary result and the middle is a compromise.

---

14 Attic black figured fragment KHM ANSA IV 4594c, unpublished.
15 KHM ANSA IV 3598; ABV 335.4; CVA-Online 301827. So far the attic geometric pitcher KHM ANSA IV 3452 is unpublished.
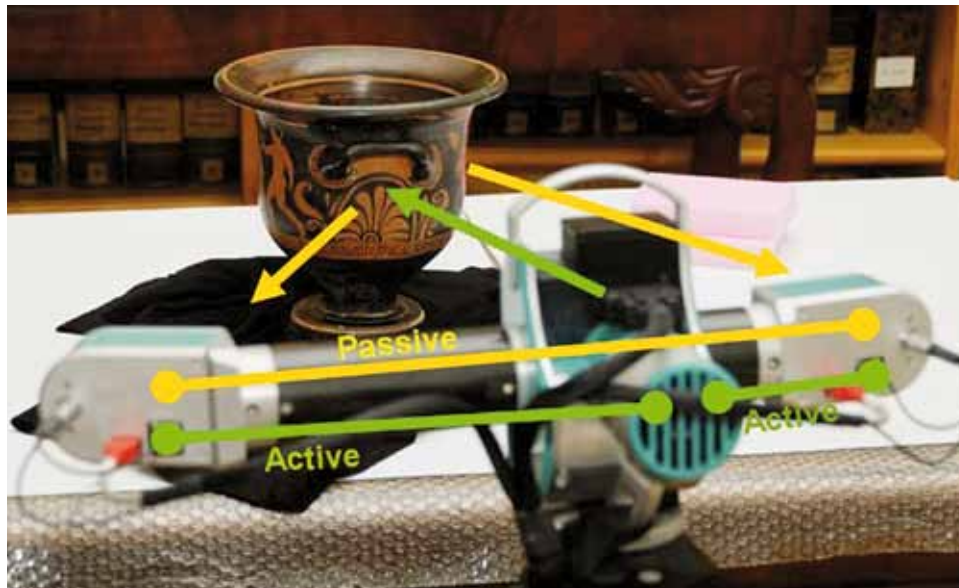
Figure 2: *Krater* UMJ Inv. Nr. 4611 and the scheme of the two active 3D-scanners and passive stereo system of the *Breuckmann smartSCAN-3D-HE*.

The *smartSCAN* uses optics with a fixed focal length, therefore it requires a wider selection of optics than the *Vi-9i* with a variable focus in order to cover all object sizes. Changing and calibrating the optics of a 3D-scanner requires 10–20 minutes, which led to the decision to acquire the objects sorted by a mixture of size first and shape second. The benefit of this mixture is a minimum of delays for changing optics and maximizing the routine for the handling of objects of the same shape.

Comparing the *smartSCAN* to the *Vi-9i* and its recent successor the *Range5*[16], the *smartSCAN* has distinct advantages in respect to color and accuracy, because it uses 5.0 megapixel color cameras instead of a 3.0 (1.0 for the *Range5*) megapixel monochrome camera. It has to be noted that the newer *Range5* has no color acquisition, unlike the *Vi-9i*, which had a color filter wheel in order to gather a red, green and blue texture-map. Therefore, the rollouts shown in Section 4 could only be done for the 3D-models acquired in 2009.

Another feature, which has proven to be important for cuneiform tablets[17] is the fact that the *smartSCAN* consists of three 3D-scanners in the High-End (HE) configuration using two cameras and a light projector in the middle. Each camera paired with the projector is an active 3D-scanner using the principle of structured light. The two cameras without the projector act as a passive stereo system. Figure 2 shows the scheme of the three 3D-scanners included in the *smartSCAN-3D-HE* using the 470 mm FOV and the *krater* Inv. Nr. 4611[18] of the *Universalmuseum Joanneum* (UMJ) Graz.

For the Breuckmann *smartSCAN-3D-HE* a wide range of different optics exists, which is categorized by the range image diagonal (FOV) and not the focal length. For many archaeological finds the FOV of 150 mm has proven to be the best choice in order to acquire small details such as fingerprints. When objects contain even smaller details, such as seal imprints and toolmarks, the FOV with 60 mm is recommended. The FOVs of 470, 600 and 1000 mm are suitable for acquiring larger objects such as reliefs and statues and can also be used for scanning whole temples.[19] For flat objects, such as a fragment of the bottom of a vessel, a comparison with flat bed scanners can be roughly estimated in Dots Per Inch (DPI) by dividing the cardinality of the measuring points (vertices) by the acquired surface (in square *inches*) of the resulting 3D model. By using a 3D-scanner based on 5.0 megapixels cameras we can achieve ≈ 1000 DPI for the FOV of 60 mm, ≈ 300 DPI for the FOV

---

[16]   Practical tests were done in spring 2009 at the IWR, Heidelberg University together with Konica-Minolta.
[17]   Mara et al., GigaMesh.
[18]   Katalog Archäologiemuseum, Fig. 1068; A. D. Trendall, The Red-figured Vases of Apulia 1 (Oxford 1978) 160 Nr. 206.
[19]   Cf. fn 5.

Figure 3: Setup of the 3D scanner and the *turntable* for the acquisition of KHM ANSA IV 3601. The image on the top shows a *Breuckmann smartSCAN-3D-HE* using the optics with a *FOV* of 470 mm. The lower images show the structured light patterns projected on the object during the acquisition.

of 150 mm down to ≈ 100 DPI for the larger FOVs. Recently a FOV of 35 mm has been added for forensic sciences, which pushes the resolution up to ≈ 2,500 DPI – equaling a spatial resolution within the 10 µm-range.

Figure 3 shows the *smartSCAN-3D-HE* during acquisition using the 600 mm FOV for an *amphora* in the KHM[20] and the projected structured light patterns. The whole acquisition process requires less than 5 seconds depending on the shutter time. The object is placed on a *turntable* to acquire pre-registered 3D-scans. Depending on the shape of the object and its applications like handles, the *turntable* is rotated about 30˚ to 60˚ to gather 6 to 12 3D-scans. In the case of objects with a more complex shape than vessels, the *turntable* can be rotated to an arbitrary number of positions and angles.

In summary it can be noted that the industrial grade 3D-scanners were well suited for the CVA project, especially when color information can be gathered by the 3D-scanner itself. This is useful for the acquisition and post processing, as shown in the next section, and it enables the computation of more complex visualizations, such as rollouts, shown in section 4.

2.2   Acquisition Process and Post Processing

The acquisition of an object consists of several steps. In the following, we give an overview of our experiences and techniques concerning the recent CVA volume. The values in Table 1 give a first clue about time and further effort for typical CVA objects. Generally, it is difficult to determine an average acquisition time for

---

[20]   KHM ANSA IV 3601; ABV 394.8; CVA-Online 302947.

the vessels, because it depends on the number of required scans which on their part again depend on the size, shape and surface condition of the object, as well as on the ambient light.

		fragment	lid	vessel	total
# objects		20	15	86	121
acquisition time	total [h]	10.2	11.7	81.9	103.8
	average [min]	31	47	57	51
# partial scans	total	247	375	2561	3183
	average	12.35	34.1	28.1	26.1
# vertices	average	690670	821976	965354	901116
# faces	average	1370237	1639234	2069171	1897509
file size	average [MB]	27.36	32.55	38.13	35.62

Table 1: Total numbers of 3D-scans, measuring points (vertices), file sizes and acquisition times for the objects of the recent CVA volume (CVA Wien 7). The given file size is computed using the *Stanford PLY* binary file format of the post-processed 3D-models.

It takes several single scans (see Table 1) to acquire the whole surface of an object. A single scan consists of one or multiple grabs. A grab is a single shot with a fixed illuminance intensity and shutter speed. Comparable with High Dynamic Range Images (HDRI)[21], one scan can be composed of multiple grabs – each with a different illumination – if a fixed illumination would yield too much over and underexposed surface areas, which constrain the data acquisition. This may occur for vessels whose surface is partly glossy black and partly matt finished pale. This wide color and specular range cannot be covered by one grab, thus different grabs with different illumination intensities are required. Nevertheless, it remains difficult to capture the transition areas between the different surface qualities where discontinuities may occur, in spite of manually adjusted multiple grabs.

Using multiple grabs influences the acquisition time for a single scan. The scanner needs between 5 and 10 seconds for one grab. Additionally, the acquisition time increases by the time that is needed to adjust the illumination settings by the user. In general, exposition settings are chosen which allow acquiring as much of the surface as possible with one single scan.

Another factor determining the scan amount is the shape of the vessel. As shown in Figure 1, only surface areas that can be "seen" by both cameras (and/or the projector) can be acquired.

Additionally, the time for pre-aligning the single scans influences the total acquisition time. The pre-aligning process during the scan procedure is important, because it provides a preliminary orientation for the user as to which surface areas have not been scanned yet. A single scan has to overlap sufficiently (at least about 10%) with the previous scans so that the scans can be aligned. The aligning process can be accelerated manually by providing good initial values. This is done by selecting corresponding vertices on the additional scan and on the previous scans. For identifying these pairs the color values that the scanner acquires are an important tool, because they offer an orientation for the user. The pre-aligning process has to be accomplished with every further single scan.

If it is possible to use a rotating turntable to place the object on, the amount of manual aligning can be minimized; only the first two scans have to be aligned manually. From this, the rotational axis can be computed and all further scans are aligned automatically, as long as the position of the scanner and the object's position (except for the rotation of the turntable) do not change. If that happens however, the aligning process has to be repeated manually.

21 E. Reinhard – G. Ward – S. Pattanaik – P. Debevec, High Dynamic Range Imaging: Acquisition, Display, and Image-Based Lighting (San Francisco 2005).

Using a turntable is a good solution for damageable objects, because it reduces the manual handling of the object. Most of the vessels that were scanned in the course of the CVA projects had only to be moved manually five times:

1. putting the vessel on the turntable
2. turning it upside down (if possible)
3. laying it on one side
4. laying it on the other side
5. removing it from the turntable.

After the acquisition process, the data has to be post processed. This includes "cleaning" the meshes, i.e. removing acquired parts of the environment that do not belong to the scanned object, as well as the precise alignment of the partial scans and creating a mesh. The same amount of time that is needed for the acquisition can be expected for the post processing. It takes about 20 minutes per object to create profile lines, silhouettes and side views in such a way that they can be further processed by an archaeologist.

3   PROFILE LINES FROM 3D-MODELS

This section shows how profile lines and silhouettes can be computed from the 3D-scanned data, instead of being drawn by hand.

3.1   Rotational Axis

To compute the profile and silhouette lines of a vessel, one needs to define an intersection plane. This intersection plane contains an estimated rotational axis of the vessel. Since the vessels are handmade they do not have a single well-defined rotational axis. There are different possibilities to choose or determine *one* rotational axis. We have to distinguish between rotational axes that are specified by the vessel's base, as shown in Figure 4 a, and a rotational axis that is determined by the vessel's corpus, as shown in Figure 4 b and 4 c.

If it is significant for the project to determine the rotational axis of complete vessels correctly by using 3D-models, this should be done on segments of objects, because they may be manufactured in separate parts, where each part has its own axis of rotation not necessarily aligned with the axis of other parts.[22]

3.2   Silhouette and Profile Lines

Profile lines of vessels can be extracted directly from the 3D models (similar to those of fragments, as described by Kampel and Mara[23]). A plane is inscribed into the model and its intersection with the mesh yields the polygonal chain that can be exported. Also, the silhouette can be gained by adjusting a plane parallel to the intersection plane (e.g. the intersection plane itself) and orthogonal to the viewer's direction and then exporting the outer mesh edges of the 3D model. These polylines can be saved and processed further.

3.3   Data Formats for Profile Lines

There are different possibilities for saving this polygonal chain digitally: As a picture, i.e., a bitmap with a certain resolution, or as a vector graphic. For the latter, the coordinates of the vertices of the polygonal chain are saved. Hence, the points' relative positions are given independently from a certain resolution. In Figure 5 the difference between the two representations is clarified by a scale-up of a profile line.

---

[22]   H. Mara – R. Sablatnig, Determination of Ancient Manufacturing Techniques of Ceramics by 3D Shape Estimation, in: H. Zha – Z. Pan – H. Thwaites – A. C. Addison – M. Forte (ed.), Proc. of the 12th International Conference on Virtual Systems and Multimedia (VSMM), Xi'an, China, October 2006 (Berlin, Heidelberg 2006) 349–357.

[23]   H. Mara – M. Kampel, Automated Extraction of Profiles from 3D Models of Archaeological Fragments, in: M. O. Altan (ed.), Proc. of the XIXth CIPA International Symposium: New Perspectives to Save Cultural Heritage, Antalya, Turkey, 2003 (Istanbul 2003) 87–93.

Figure 4: Different possibilities to determine the rotational axis of a vessel (KHM ANSA IV 1132). Since the vessels are handmade, there might be imperfections in symmetry. (a) The rotational axis is orthogonal to the base, thus the axis does not fit to the corpus. (b) The corpus of the vessel specifies its rotational axis, thus the axis does not fit to the base.
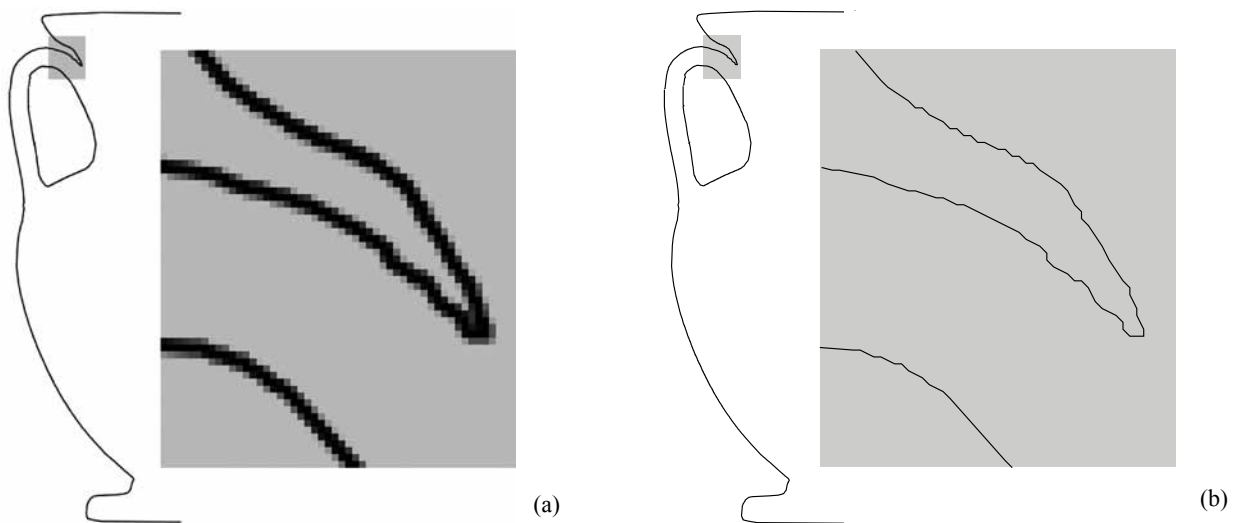

Figure 5: The difference between raster graphic and vector graphic is visible in closer examination. This is shown here at a computationally acquired silhouette line of a vessel (KHM ANSA IV 670). (a) Raster graphic: The details show that with a fixed resolution the polyline cannot be scaled up arbitrarily without losing its precision. (b) Vector graphic: The polyline is scalable since this graphics representation does not depend on a certain resolution.

Apart from being independent from resolution, another advantage of using vector graphics is the fact that they provide an easier and clearer further processing, e.g. being smoothed or compressed as described by Portl.[24]

Figure 6 a shows a manual drawing of a vessel in comparison to the silhouette and profile line computed by the acquired 3D-model, shown in Figure 6 b. The manual drawing contains all details like hatchings as used

---

[24] J. Portl, Subdivision curve and surface fitting for mesh compression (Thesis, Heidelberg University, 2010).
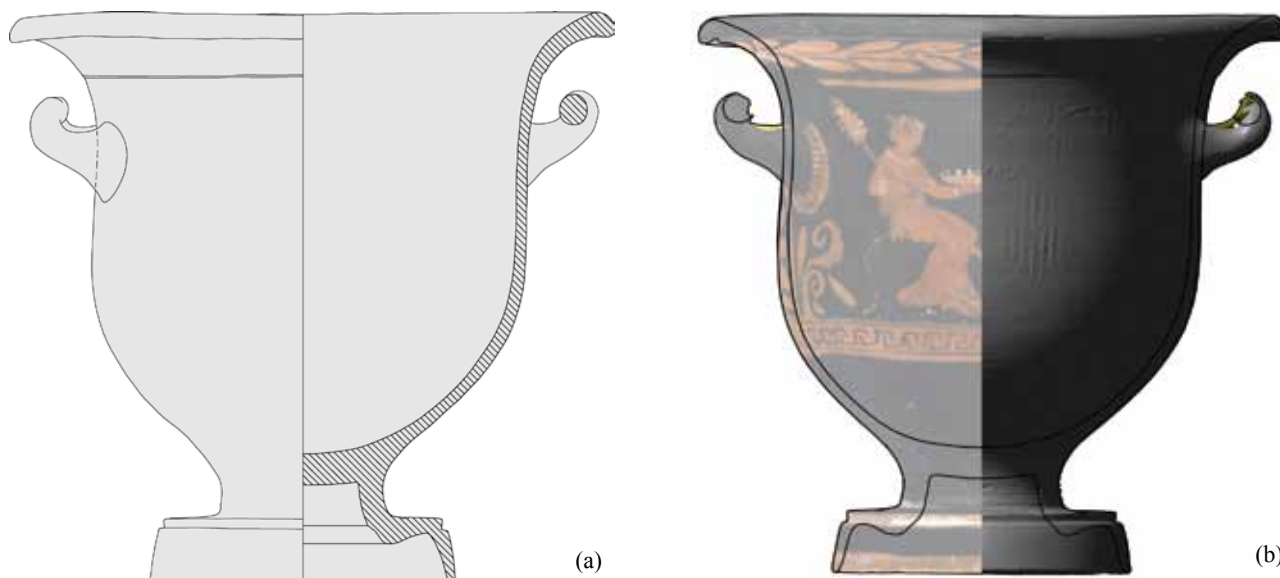
Figure 6: Front view of UMJ Inv. Nr. 4611: (a) Manual drawing by Stephan Karl. (b) Silhouette, profile and 3D-model with/without texture map and illumination.

for publication. These details have to be added to the automatically computed drawing, which has additional layers of visualization of the object with and without texture-map assisting the draftsperson.

4 VIEWS AND ROLLOUTS

The profile line and the silhouette are important for schematic drawings of vessels and are well suited to publish larger amounts of objects such as coarse ware. As the objects of the CVA projects are ornamented and these decorations had been acquired by the 3D-scanner, we had to provide additional means of visualizations. Therefore, we rendered additional images, which act as draft layers for the final publication, with the benefit of being true-to-scale and using the 3D-models. The simplest method is orthographic projection (also known as parallel projection). In contrast to photographs there is no perspective distortion and no blurring from depth of field. Additionally, we can visualize the objects with or without light. The latter is equal to an ideal ambient illumination. Furthermore, we can discard the texture-map to show only the geometry of the object. Figures 7 a–b show the principle of projecting views on the bounding box; the visualization without texture-map is shown in Figure 7 c. The bounding box of a 3D-model of an orientated vessel is a rectangular cuboid enclosing the object. The lengths of the edges of this enclosing box correlate to the maximum dimension in x-, y- and z-direction of the object.

Figure 8 shows the view from the top, all of the side views and the bottom view of the same object. This arrangement is a variant of the so-called *fat-cross*.[25] These images show color variations along the surface, because, due to time constraints, we used the projector for the patterns of the 3D-scanner to acquire the texture-map. If a better color representation is required, flash lights and studio illumination as used by photographers can be added and triggered by the 3D-scanner, as shown in the manual of the *smartSCAN-3D-HE*. In this case, the flash lights should be arranged in order to minimize shadows, just as in photography.[26] The reason to apply a maximum of homogenous illumination is that any shadow in the Field of View of the 3D-scanner will be permanently added to the texture-map of the 3D-model.

As we chose not to manipulate the acquired 3D-data, parts of the 3D-model are missing. This is either shown by white spots of the background color or the red-gray color of the backside of the triangles describing

---

[25] Mara et al., GigaMesh.
[26] Details about using flash photography in combination with 3D-scanners can be found in M. Dellepiane – M. Callieri – M. Corsini – P. Cignoni – R. Scopigno, Improved Color Acquisition and Mapping on 3D Models via Flash-based Photography, Journal on Computing and Cultural Heritage (JOCCH), 2(4), February 2010, 1–23.
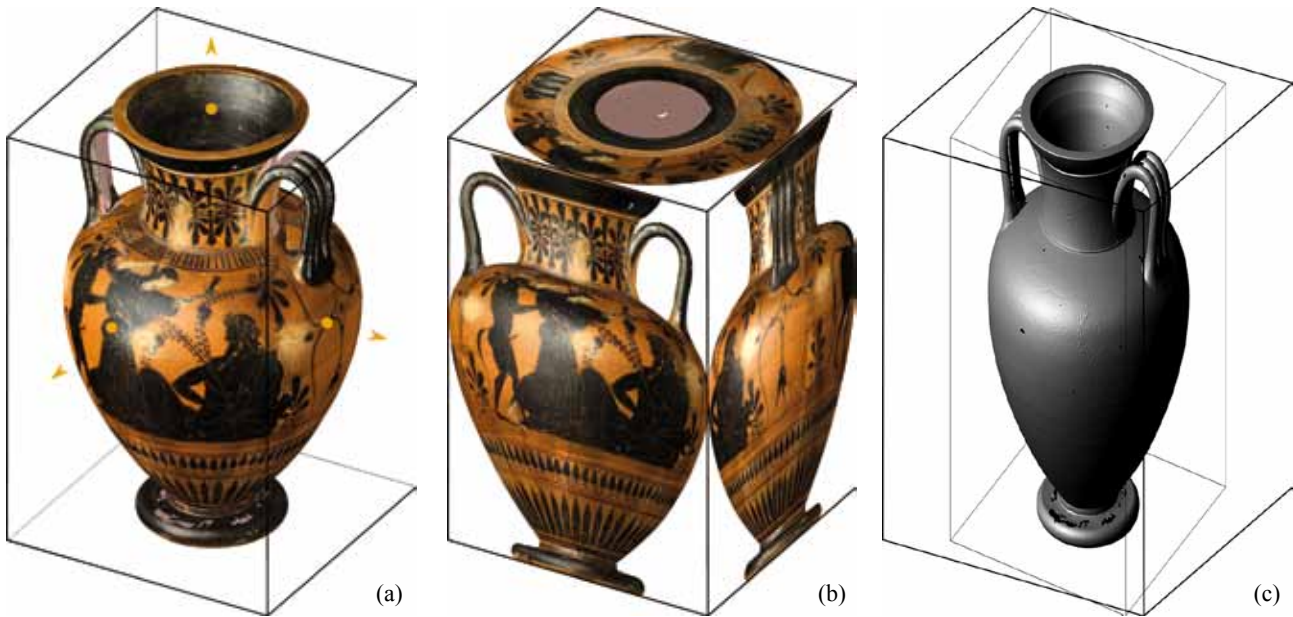
Figure 7: (a) Isometric view and bounding box of KHM ANSA IV 3601. (b) Front, side and top-view of the vessel projected on its bounding box. (c) Isometric view without texture-map.

the surface – also called backface color. The top-view of the *amphora* shows that the part of the orifice was acquired, but the bottom of the interior part of the surface is missing.

The images shown in Figure 8 are not only parallel projections using a single screenshot with e.g. 1024 × 768 pixels, they were also rendered with a specific scale, e.g. 100 DPI with 1100 × 1700 pixels for the side views. This allows us to print these images with 1000 DPI in a scale of 1:10 with a dimension of 28 × 43 cm, which equals 11 × 17 inch.

Figure 9 shows a schematic drawing of the 1024 × 1024 *pixels* tiles used to render a *pinax* in the Kunsthistorisches Museum[27] with 400 DPI. The maximum of the squared tile size in pixels depends on the graphics card of the computer used for rendering, which does not exceed 4096 × 4096 *pixels* for present-day hardware. As these tiles contain unnecessary white space, the final raster image is cropped. For the *pinax*, the raster image is cropped from 7168 × 5120 *pixels* to 7032 × 3560 *pixels*.

In addition to the parallel projections, we can use other methods well-known from geometry and cartography for our 3D-models in order to visualize the ornaments on convoluted surfaces, as shown in the next section.

4.1   Unwrapping Primitives

The surface shape of a vessel can be approximated by a combination of different rotational symmetric geometric primitives, such as cylinders (see rollouts of Nasca ceramics[28]), cones, conical frustums, spheres and spherical segments. Conical frustums and cylinders can be unrolled and therefore projected to the plane without any distortions. Other surfaces such as spherical segments can also be projected to the plane, but the image will be distorted depending on the projection method, as shown below. After fitting one of these auxiliary primitives to the model, the transformation that maps the primitive in the plane is applied to the 3D model of the vessel. An orthographic projection yields the complete rollout image.[29]

---

27   KHM ANSA IV 4398; K. Gschwantler – W. Oberleitner, Götter, Heroen, Menschen. Antikes Leben im Spiegel der Kunst, Sonderausstellung der Antikensammlung (Wien 1974) Nr. 109 fig. 20; H. Mommsen, Exekias I. Die Grabtafeln, Kerameus II 11 (Mainz 1997) 28 fn. 238.

28   Cf. Fn. 9.

29   For details about the mathematical solutions for rollouts and technical implementation see Bechtold et al., Rollouts.

Figure 8: Parallel projections of KHM ANSA IV 3601 from left to right, top to bottom: view from the top; side A seen from the left, front and right hand side; side B and view from the bottom. This representation is also known as *fat-cross*. The images are true-to-scale.
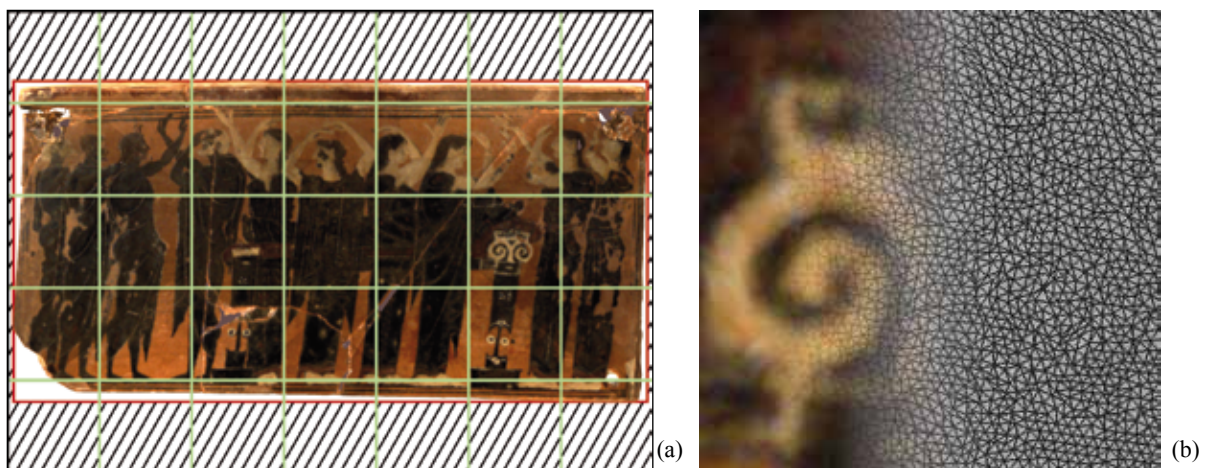

(a)

(b)

Figure 9: KHM ANSA IV 4398 with a width of 44.6 cm and a height of 22.6 cm. (a) rendered as a raster graphic with 400 DPI (when printed scaled 1 : 1) using 7 × 5 tiles. The striped area is the white space cropped from the raster image. (b) Enlarged detail of the tile in the third row and sixth column showing the texture-map and the triangles of the 3D-model.

Figure 10: Schematic illustration of creating the rollout of a vessel (KHM ANSA IV 3618) that can be approximated by conical frustums and its distortion-free rollout.

Figure 11: Illustration of a surface of a vessel approximated by a sphere and its distorted rollout.

It is difficult to approximate bellied vessels by conical frustums. Their curved silhouette would require several frustums in order to approximate the shape, but this would discerp the frieze. Generally, multiple frustums for one vessel are only reasonable if the frieze itself is partitioned (as in Figure 10). A sphere or spherical segments (Figure 11) can be fitted into bellied vessels. Their disadvantage compared to frustums is that they are undevelopable surfaces, so they cannot be unrolled without distortion. There are many techniques, originally from map projection, which transform the sphere surface into a plane. None of them are able to preserve the angle as well as the relation among the lengths and areas at the same time.[30]

As head-shaped vessels and other mold-made vessels cannot be represented through a reasonable number of geometric primitives, each of these vessels has to be treated separately or represented by orthographic views.

Generally, the rollouts can be computed using tiled rendering, which yields the possibility to produce full-scale rollouts.

5   ESTIMATION OF VESSEL VOLUMES

Determining the capacity of transport vessels is important in order to study ancient measuring systems as well as trading relations. M. Hüttig[31] demonstrates how to estimate the inner volume for *amphorae* using traditional methods by rotating the inner profile line, which lead to solids of revolution.[32] Additionally, Hüttig estimates the expected error using drawings, photographs and various filling materials. The errors given in this work range between 10% and 20%; this is often not sufficient in order to draw an archaeological conclusion.

An alternate and more precise error estimation can be found: the inner volume of vessels is computed using *Computed Tomography* (CT) data and compared to repeated measurements using rice and water.[33] D. Jungblut shows that the best choice for capacity estimations are CTs, as they always provide the inner surface of any vessel and therefore have no measurable error. However, CTs[34] have several drawbacks in processing larger quantities of vessels as well as for large vessels and they do not acquire any color information required for rollouts – as shown in the previous section.

The method shown for CT data can be adopted directly for 3D models of open vessels. For closed vessels, the inner surfaces are only partially available. This led to the decision to estimate the missing regions by using the wall thickness of the partial surfaces and *a priori* knowledge from fragmented vessels. The estimation is achieved by so-called offsetting a copy of the outer surface of the vessel in the negative direction. The result is an estimate of the inner surface. The offset was given as a range of values based on broken reference objects provided by archaeologists.

As the filling level corresponds to the capacity, we decided to compute the capacity by using the vessel's orifice surfaces and the most likely filling level given by archaeologists. For some vases in the KHM we computed the maximum and minimum capacity for each of the possibilities of wall thickness. The result was a table

---

[30]   The different techniques and their application on Attic vessels are described in Bechtold et al., Rollouts and E. W. Grafarend – F. W. Krumm, Map projections (Berlin, New York 2006).
[31]   Hüttig, Methoden.
[32]   J. W. Harris – H. Stocker, Handbook of Mathematics and Computational Science (New York 1998) 576.
[33]   Jungblut, Rekonstruktion, 218–223.
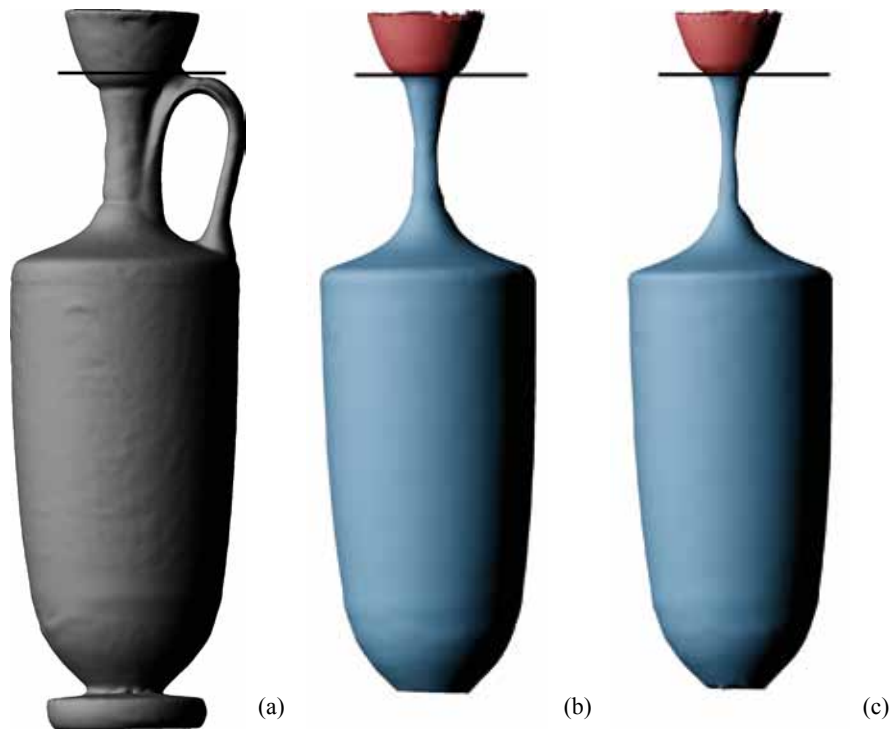[34]   See S. Karl – D. Jungblut – J. Rosc in this volume.

Figure 12: KHM ANSA IV 3746's (a) outer surface enclosing a displacement volume
of 1269.3 cm³ with the orifice planar closed, (b) inner surface with an offset
of 4 mm enclosing 950.2 cm³/919.5 cm³ and (c) inner surface with an offset
of 6 mm enclosing 842.8 cm³/817.6 cm³. The second capacity (in b and c) is
computed using the most likely filling-level shown as a black line.

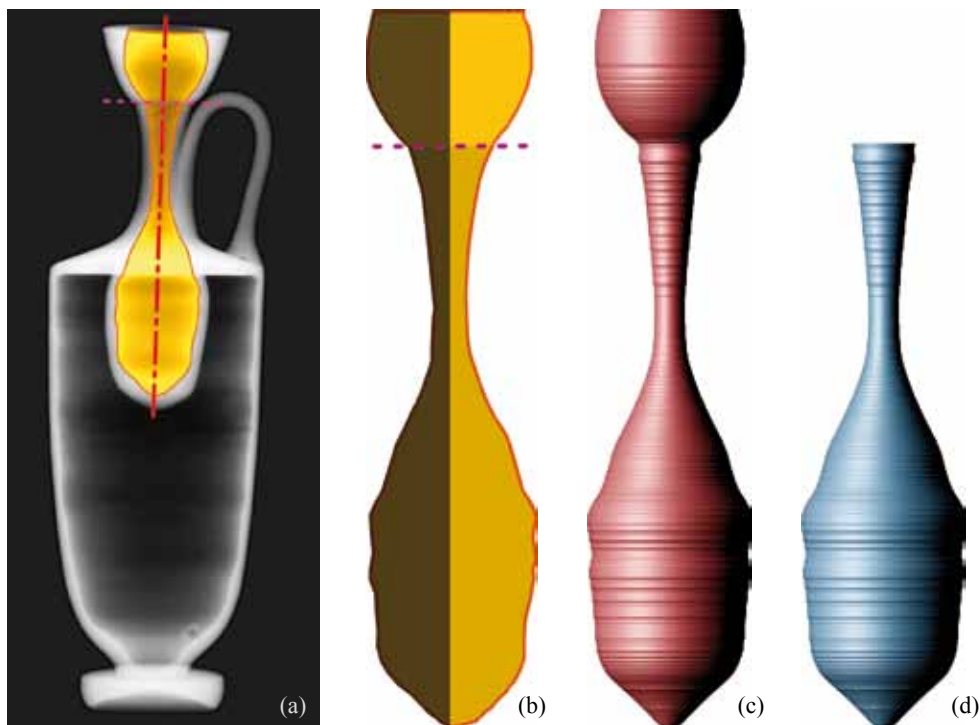Figure 13: (a) X-Ray raster image of KHM ANSA IV 3746 with a false bottom marked in yel-
low. The vertical line shows the rotational axis of the compartment. The horizontal line
shows the assumed filling level. (b) Raster image of the false bottom – the left half is
used to compute the volume and a 3D-model by rotation of the outline, (c) for the com-
plete compartment and (d) for the filled compartment.

with typically two by two entries, indicating the range of the most likely capacity.[35] For cross-validation and future reference we also computed the outer (displacement) volume of each vessel, also using the orifice surface.

Figure 12 a shows the outer surface of a white ground *lekythos*[36] and its assumed filling level. The following computations were done neglecting the false-bottom in order to get an impression on how much content the vessel appears to contain. Using the outer surface and closing the orifice, the vessel encloses a displacement volume of 1269.3 cm³. Figure 12 b and c show the inner surface computed by an offset[37] of 4 mm and 6 mm having a maximum capacity – filled up to orifice – of 950.2 cm³ and 842.8 cm³. Using the supposable filling level shown as a black bar, the volume of the capacity computes to 919.5 cm³ and 817.6 cm³.

5.1 Vessels with False Bottom

Vessels with false bottoms – i.e. special compartments (*Einsatzbehälter*) – were acquired by using X-ray. For each of these vessels, one X-ray image was taken, with the vessels orientated as used for the profile section estimation.[38] The X-ray images are raster images with a minor perspective distortion similar to regular photographs. As we only made one image per vessel, we can compute the outline of the compartments as shown in Figure 13 a–b. In general, the X-ray image has no scale, which is however required in order to compute an absolute volume in cm³ by using the outline. Because the profile line is on the same plane as the compartment's outline within the X-ray image and we know the exact height and width of the profile line, we can use these dimensions to compute a scale. This is done by dividing the width and height of the profile line in pixels by the width and height from the profile line of the 3D-model. The result is a scale in pixel per cm, which can be converted by multiplication of 2.54 inch/cm into *Dots Per Inch* (DPI), when needed.

Using the scale, we can assign a radius and a height for each pixel row of the compartment's outline. Rows with the same radius can be stacked together, thus describing a cylinder with a height computed by using the number of pixels and the scale. Therefore we can compute the volume of the compartment as sum of the volume of all cylinders. This method is known as Cylinder Method or Shell Integration.[39] Figures 13 c–d show the 3D-model of the false bottom consisting of cylinders. Figure 14 shows a detail of the pixel rows of the X-ray image and the corresponding cylinders of the 3D-model.

The computed capacity for the false bottom of the white ground *lekythos* already mentioned above is 80.1 cm³ when it is completely filled. Using the filling level shown in Figures 13 a and b, the capacity is 57.9 cm³. Therefore, we can compute the ratio between the used capacity and the capacity the vessel appears to have. This is shown in Table 2.

filling level	wall-thickness	
	4 mm	6 mm
assumed	6.3 %	7.1 %
orifice	8.4 %	9.5 %

Table 2: Capacity of the false-bottom in respect to the same vessel neglecting the false-bottom.

---

[35] H. Mara – E. Trinkl – P. Kammerer – E. Zolda, 3D-Acquisition and Multi-Spectral Readings for Documentation of Polychrome Ceramics in the Antiquities Collection of the *Kunsthistorisches Museum* Vienna, in: J. Trant – D. Bearman (ed.), Proc. of the International Cultural Heritage Informatics Meeting (ICHIM '07), Toronto, Ontario, Canada, 2007 (CD–ROM) <http://www.archimuse.com/ichim07/papers/mara/mara.html> (8.4.2011); CVA Wien 5, p. 134 f.

[36] KHM ANSA IV 3746; ARV² 998.164; CVA Wien 5 pl. 69; CVA Online 213987.

[37] S.-J. Kim – D.-Y. Lee – M.-Y. Yang, Offset Triangular Mesh Using the Multiple Normal Vectors of a Vertex, in: Proc. of CAD '04 Conference, Pattaya, Thailand, 2004, Computer-Aided Design 1 (2004) 285–291.

[38] See B. Vak in this volume.

[39] H. Anton, Volumes by Slicing; Disks and Washers, in: Calculus with Analytic Geometry ²(New York 1984) 359–367 (§6.2). An example for the application in the field of archaeology can be found in Hüttig, Methoden.
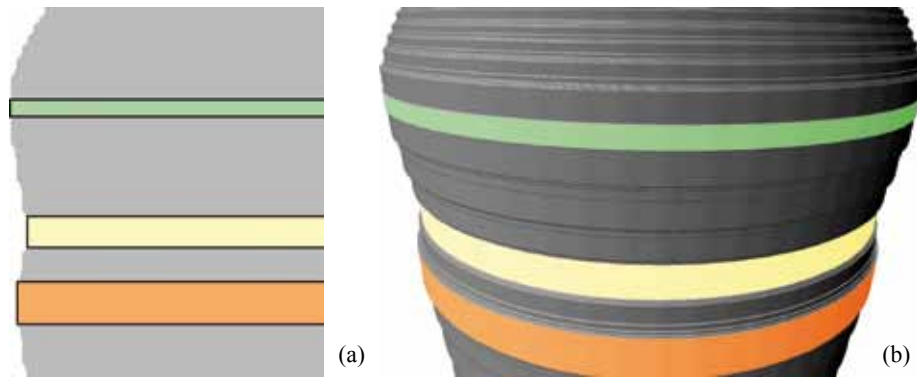
Figure 14: (a) Enhanced detail of the X-Ray raster image of KHM ANSA IV 3746 with pixel
             rows of equal radius marked in color. Using the calibrated scale of the raster image,
             the real radius of the virtual cylinders can be computed. (b) Shows the correspond-
             ing cylinders in the 3D-model.

6   SUMMARY AND OUTLOOK

Summarizing the work based on close-range 3D-acquisition, we could show that all the measurements for the profile drawings and rollouts can be achieved within three to four weeks for ca. 120 vessels for each of the two recent Viennese CVA volumes. Nevertheless we have to stress the fact that for 3D-acquisition the number of actual objects and fragments as well as their complexity determine the acquisition time. For example a vase with a highly decorated lid [40] will take almost twice the time than a regular vase. On the other hand, a large and bulky vessel like a *dinos* can be acquired in half of the time of a much smaller head-shaped vessel (*Kopfgefäß*).

Even given the fact that views and profile lines computed directly from the 3D-models have flaws such as gaps, the process of providing a publication ready drawing as well as the accuracy of the drawings could be dramatically improved. Further benefits are: no lens distortion as known from photography; contact-free and radiation-free acquisition; the views and rollouts can be computed as true-to-scale high-resolution images, only limited by the resolution of the chosen FOV. As our software tools are independent from the 3D-scanners hardware, we will be able to achieve an even higher amount of details for the documentation of visualization with the next generations of 3D-scanners. This includes all other extra information we can gain from 3D-models such as volume estimation and pin-pointing multi-spectral readings. [41]

Future work will enable the automatic extraction of meaningful features in vector representation similar to the ongoing work on cuneiform extraction. [42] The result will be an even faster work flow minimizing the post processing of drawings for publication. Features such as photographic details or manufacturing traces as well as automated, objective and digital comparison will be available.

[40]   E.g. KHM ANSA IV 1; B. Kratzmüller in: Jahresbericht KHM 2008, 49 (Fig.).
[41]   Mara et al., Acquisition; see also P. Kammerer – F. Mairinger – E. Trinkl – E. Zolda in this volume.
[42]   Mara et al., GigaMesh.